A TRIDENT SCHOLAR PROJECT REPORT

NO. 509

Parametric Analysis and Optimization of an Elastocaloric Refrigeration Cycle

by

Midshipman 1/C Sarah M. Nguyen, USN

UNITED STATES NAVAL ACADEMY
ANNAPOLIS, MARYLAND

USNA-1531-2

REPORT DOCUMENTATION PAGE

Form Approved
OMB No. 0704-0188

1. REPORT DATE *(DD-MM-YYYY)*	**2. REPORT TYPE**	**3. DATES COVERED** *(From - To)*
7/12/21		

4. TITLE AND SUBTITLE
Parametric Analysis and Optimization of an Elastocaloric Refrigeration Cycle

5a. CONTRACT NUMBER

5b. GRANT NUMBER

5c. PROGRAM ELEMENT NUMBER

6. AUTHOR(S)
Nguyen, Sarah, M.

5d. PROJECT NUMBER

5e. TASK NUMBER

5f. WORK UNIT NUMBER

7. PERFORMING ORGANIZATION NAME(S) AND ADDRESS(ES)

8. PERFORMING ORGANIZATION REPORT NUMBER

9. SPONSORING / MONITORING AGENCY NAME(S) AND ADDRESS(ES)
U.S. Naval Academy
Annapolis, MD 21402

10. SPONSOR/MONITOR'S ACRONYM(S)

11. SPONSOR/MONITOR'S REPORT NUMBER(S)
Trident Scholar Report no. 509 (2021)

12. DISTRIBUTION / AVAILABILITY STATEMENT

This document has been approved for public release; its distribution is UNLIMITED.

13. SUPPLEMENTARY NOTES

14. ABSTRACT

Elastocaloric heating/cooling takes advantage of the structural changes in shape memory alloys (SMAs) that release and absorb heat when a strain is applied over a transition temperature. Heating/cooling cycles that use SMAs offer a potential solution to issues associated with the use of ozone-depleting refrigerants found in common heat pump/refrigeration cycles. Several recent works have found that the Coefficient of Performance (COP) for elastocaloric cycles is comparable to those achieved with standard HVAC systems of the same scale, which exhibit COPs of 3 on average. Conversely, SMA wires in lab settings have shown to achieve COPs as high as 3.5, and with sufficient optimization are expected to achieve COPs greater than 10. This study will be a continuation of the work performed by Sharar et al. (Army Research Lab), which established a first-of-its-kind solid-state continuous flow loop using nitinol (NiTi) wire. In this work, we explore the parametric space for optimization of Sharar's cycle using COMSOL Multiphysics (v. 5.5) to model the behavior of NiTi (an SMA) as strain is applied and released around a bend, where heat absorption and release occurs. We perform a parametric study that varies the wire radius, disk radius, its rotational speed, and its contact area with the primary heat sink to subsequently optimize its performance and to identify the parameters that will maximize COP, endothermic temperature change, and cooling power.

15. SUBJECT TERMS
Elastocalorics, martensitic transformation, shape memory effect, superelasticity, nickel titanium

16. SECURITY CLASSIFICATION OF:			**17. LIMITATION OF ABSTRACT**	**18. NUMBER OF PAGES**	**19a. NAME OF RESPONSIBLE PERSON**
a. REPORT	**b. ABSTRACT**	**c. THIS PAGE**		32	**19b. TELEPHONE NUMBER** *(include area code)*

U.S.N.A. --- Trident Scholar project report; no. 509 (2021)

PARAMETRIC ANALYSIS OF AN ELASTOCALORIC REFRIGERATION CYCLE

by

Midshipman 1/C Sarah M. Nguyen
United States Naval Academy
Annapolis, Maryland

Certification of Advisers Approval

Associate Professor Ronald J. Warzoha
Mechanical Engineering Department

Professor Andrew N. Smith
Mechanical Engineering Department

Professor Joshua J. Radice
Mechanical Engineering Department

Associate Professor Brian F. Donovan
Physics Department

Acceptance for the Trident Scholar Committee

Professor Maria J. Schroeder
Associate Director of Midshipman Research

USNA-1531-2

Abstract

Elastocaloric heating/cooling takes advantage of the structural changes in shape memory alloys (SMAs) that release and absorb heat in response to an induced strain. Heating/cooling cycles that use SMAs offer a potential solution to issues associated with the use of ozone-depleting refrigerants found in common heat pump/refrigeration cycles. Several recent works have found that the Coefficient of Performance (COP) for elastocaloric cycles is comparable to those achieved with standard HVAC systems of the same scale, which exhibit COPs of 3 on average. Conversely, SMA wires in lab settings have shown to achieve COPs as high as 3.5, and with sufficient optimization are expected to achieve COPs greater than 10. This study is a continuation of the work performed by Sharar et al. (Army Research Lab), which established a first-of-its-kind solid-state continuous flow loop using nitinol (NiTi) wire, whereby the wire rotates continuously in a loop configuration, initiating heat release and absorption when the wire enters and exits a region of curvature [13], [14]. In this work, we explore the parametric space for optimization of this cycle using both computational and experimental methods. The cycle is modeled using COMSOL Multiphysics (v. 5.5). We perform a parametric study that varies the wire radius, disk radius, rotational speed, convection coefficient over the disk, and contact resistance between the wire and disk to optimize its performance and identify parameters that maximize COP, temperature change, and cooling power. Simultaneously, a physical experiment is constructed and paired with the model to validate any trends identified in the simulation. Such insight is critical to improving the performance of these systems in small-to-medium sized heating and cooling systems. This research contributes to the use of elastocalorics in microclimate heating and cooling, and will be a novel contribution to the field of solid-state refrigeration.

Keywords: Elastocalorics, Martensitic Transformation, Shape Memory Effect, Superelasticity, Nickel Titanium

Acknowledgements

I would like to extend a great thanks to my project advisors Professor Warzoha, Professor Smith, Professor Radice, and Professor Donovan. I am extremely grateful for the guidance they have given me over the last year and a half and for the mentorship they have provided me through it all. Thank you to Professor Warzoha, Smith, and Radice for taking me under their wing and for the life lessons learned along the way. Thank you to Dr. Darrin Sharar, our collaborator at Army Research Lab, for answering all of my questions and allowing us to continue his research. Finally, a great thanks to the Trident Committee as well as the Office of Naval Research for continual support and allowing me the opportunity to pursue research at the Naval Academy.

Contents

I. Background

Vapor-compression systems are the current standard for heating and cooling spaces. Though they are advantageous in both performance and reliability, they are less ideal for smaller-scale applications. As components decrease in size, they are unable to work as effectively and efficiently (particularly the compressor), becoming more costly for the amount of heating and cooling achieved. In addition to their disadvantages in scalability, they also have negative effects on the environment and consume significant amounts of energy relative to their cooling (or heating) capacities [1]. These effects are related specifically to the refrigerants used in these systems. Many HVAC systems today use Hydrofluorocarbons (HFCs), which are known to deplete the ozone layer and to contribute high global warming potentials (GWPs) (between 1,370 and 2,100 times that of carbon dioxide) when released into the atmosphere [1]. To mitigate these effects, the United States, Mexico, and Canada have proposed legislation to phase down HFC consumption by 85% during the period between 2016 and 2033 [1]. Likewise, the European Union plans to reduce consumption by 80% by the year 2030 [1]. As a result, the need to develop and refine alternatives to HFC systems to protect the environment and achieve higher system efficiencies in medium to small scale applications is critical and a worldwide priority.

Potential non-vapor-compression systems can involve magnetocaloric, electrocaloric, or elastocaloric heating and cooling [2]. However, to compare how well they perform against each other, the performance of refrigeration and heat pump systems is quantified by a metric known as coefficient of performance, or COP. For a heat pump, the COP quantifies how much heating or cooling is achieved relative to how much work is required. Equation 1 (shown for a cooling system) reveals how this is calculated from a system's measurable results.

$$COP_{refrigerator} = \frac{Q_c}{Work} = \frac{Q_c}{Q_h - Q_c} \quad \textbf{(1)}$$

Qh refers to the heat rejected to a hot sink, while *Qc* refers to the heat removed from a space, which is a cold source. The COP of a system will be used as a numerical indication of how efficiently the system operates thermodynamically. Of these technologies, elastocalorics show the most promising characteristics, having COP values that are most comparable to traditional vapor-compression systems, which operate on average at a COP of 3 [1]. Moreover, studies have shown that they can theoretically exceed these standards (to values of about 10) under ideal loading conditions [3]. Because of the potential that elastocalorics have in small-to-medium scale applications, this study interrogates only elastocaloric systems [2].

Unlike vapor-compression systems, which rely on HFC refrigerants, elastocaloric systems take advantage of the complex material properties of shape memory alloys (SMAs) in order to achieve heating and cooling. SMAs are materials that exhibit two significant properties: the shape memory

effect and superelasticity. The shape memory effect refers to the material's ability to recover large stress-induced strains upon heating above a transition temperature [4]. Superelasticity means that above this transition temperature, the material can also recover large strains isothermally (through heating and cooling) during a load and unload cycle, often following a hysteresis loop, or process dependent on the material's history [4]. These two processes are completely reversible, meaning that the input of heat can induce strain, and vice versa. For applications in refrigeration, we are primarily interested in the SMA's ability to release/absorb heat upon loading and unloading the material.

Governing Physics

An understanding of martensitic transformation is necessary to determine how SMAs can best be applied in refrigeration and heat pump systems. Martensitic transformation is the mechanism by which heating and cooling occurs in SMAs through stress-induced phase change [5]. When an increasing external stress is applied above a material's transition temperature (or minimum temperature at which transformation can occur), the SMA reaches a critical strain at which it changes from one crystal structure to another, without breaking bonds [6]. The initial (or parent phase) is called austenite, and is present at lower stresses, smaller strains, higher temperatures, and has a cubic crystal structure [5], [6]. Conversely, the transformed phase is called martensite, and is present at higher stresses, greater strains, lower temperatures, and typically has a tetragonal crystal structure [5], [6]. This transformation is a diffusionless process governed by shear distortion of the lattice structure, meaning that the atoms do not move randomly; rather, they transition into a specific orientation along a specific plane [5] shown schematically in Figure 1. When an SMA transitions from austenite to martensite to achieve stability, entropy decreases and latent heat is released, the amount of which is dictated by the volume of material that undergoes transformation. [7]. Likewise, when the load is removed from the material, the SMA returns to its original shape (the deformation strain is completely recovered), and latent heat is absorbed in order to achieve stability.

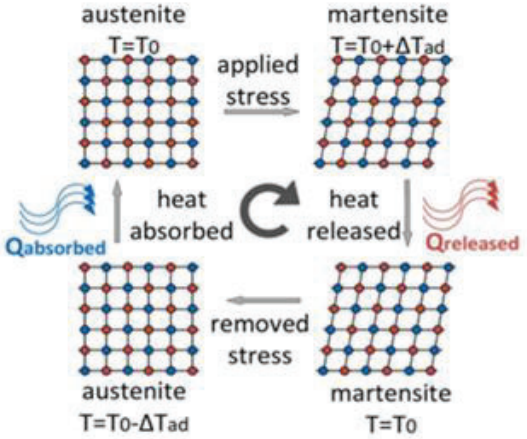

Figure 1: Diagram showing reversible martensitic transformation.

Because martensitic transformation is completely reversible, SMAs can either release heat when stress is applied, or recover a strain when heat is applied. The phase change that releases heat into the surroundings (austenite to martensite) is referred to as the exothermic transformation, while the phase change that absorbs heat from the surroundings (martensite to austenite) is called the endothermic transformation. The ability to induce this effect cyclically is what makes elastocalorics a promising candidate in refrigeration and heat pump applications. A successful system would be able to use these exothermic and endothermic reactions to allocate heat to desired locations.

The SMA that should be used for this application must have a range of desirable material properties. It must have a high latent heat associated with its stress-induced transformation, while keeping the dissipated losses during the load cycle at a minimum [8]. It must be able to resist fatigue failure without degradation of the elastocaloric effect [8]. Finally, the mechanical energy, or work input needed to initiate the phase transformation, must be significantly outweighed by the latent heat released to have a high Coefficient of Performance. Of the SMAs that meet these qualities, nickel-titanium (NiTi, or nitinol) alloys currently have the greatest potential for operational use. NiTi can exhibit large energy densities, or heat released per mass of strained material, up to and exceeding 30 J/g, and can have temperature changes between 25-58 °C [9], [10], [11], [12]. This allows the elastocaloric system to achieve COPs that are greater than its vapor-compression counterparts. NiTi is also able to recover strains of up to 10%, giving it a high reversibility of phase transformation and improving its fatigue resistance, making it a promising material for microclimate heating and cooling systems [11], [12]. Thus, the SMA studied in this research and used in the apparatus is a superelastic NiTi wire, manufactured at Fort Wayne Metals. For NiTi, the critical strain (or deformation) for transformation occurs between 1-2% strain.

NiTi Loading Curves

NiTi is an elastic-perfectly plastic material, which means that it exhibits significant elastic (recoverable) behavior up to certain loads, and significant plastic deformation past these loads. Previous research reveals that when NiTi is loaded and unloaded, its stress-strain curve is characterized by an asymmetrical hysteresis loop, where the stress required to plastically (or permanently) deform the material is greater than the stress required to plastically unload the material. Stress-strain curves produced in studies conducted by the Army Research Lab (Figure 2) demonstrate this behavior [13].

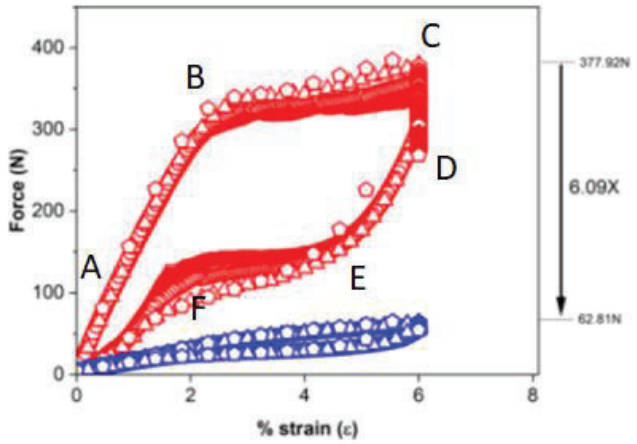

Figure 2: Force v. strain loading curve for NiTi wire. The red points are the loading and unloading data of the wire strained axially. The blue points are the loading/unloading data of the wire strain in bending. Data taken and recorded by Dr. Sharar at ARL.

As seen in Figure 2, the NiTi loading curve exhibits three areas of interest: initial linearly elastic loading (segment AB), plastic loading at an upper stress plateau (segment BC), linearly elastic unloading (segment DE), and plastic unloading at a lower stress plateau (segment EF). The linearly elastic regions of this curve describe how the material is able to recover strains based on its elastic modulus (a material property) while the plastic regions (upper and lower plateaus) characterize permanent deformation that require work to recover. These areas in particular will contribute to the amount of heat released and absorbed by the NiTi wire as it loads and unloads.

Modes of Deformation

A wire of NiTi can be loaded in two different ways: 1) axial tension/compression and 2) bending. Because the amount of heat released and absorbed by an SMA is directly related to the amount of material undergoing transformation, it is important to recognize the trade-offs between these two loading methods.

When a material is loaded along its longitudinal axis, it will experience uniform strain across its entire cross-section. Both the stress and strain distributions are constant at any location within the material. The primary benefit is that by applying a certain load, transformation can be achieved throughout the entire SMA, maximizing heat release and absorption for the material.

A material can also be loaded in a bending mode, in which case the material does not experience uniform loading or strain across its cross section. As a result, only a portion of the wire is critically strained, and will release and absorb heat. The benefit, however, is that it takes significantly less force to achieve material transformation via bending the wire rather than axially loading it (as reflected in the red and blue data sets in Figure 2). Additionally, loading the wire in a bending mode improves the ability of the wire to remove heat by extending its surface and improving

thermal contact with a fluid or a subsequent body. Because of this immense reduction in actuation force (input work) and the benefits of increased thermal contact, this study explores an elastocaloric system that takes advantage of loading an SMA via bending.

System of Interest: Elastocaloric 'Flow Loop'

The system of interest that is simulated and analyzed in this study is modelled after an elastocaloric 'Flow Loop' developed and tested at Army Research Lab (ARL) by Dr. Darrin Sharar [14]. It involves continuously rotating a wire loop of NiTi around a copper disk; the rotation of the wire is actuated by a driving disk powered by a stepper motor. This configuration takes advantage of producing a cooling power while NiTi is stressed in bending mode. By allowing the wire to 'flow' continuously into and out of the bend around the copper disk, heat release and absorption is induced cyclically.

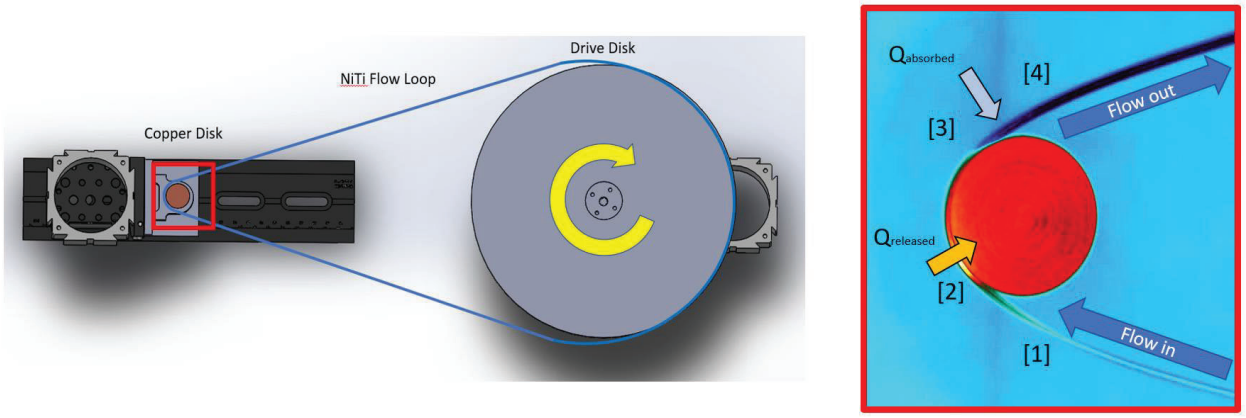

Figure 3: Elastocaloric 'flow loop' cycle and state point diagram.

The elastocaloric heating and cooling cycle takes place in its entirety as the wire rotates around the copper disk. This area is boxed in Figure 3 and is labeled with state points 1 through 4. For this apparatus, the straight sections of wire will be referred to as the unloaded state, while the curved sections will be referred to as the loaded state, and the NiTi wire exists as austenite at room temperature (25°C). At state 1, the NiTi wire, unloaded, approaches the bend at an initial temperature equal to the ambient temperature. When it reaches state 2, the wire becomes strained upon bending and releases heat through exothermic transformation. As a result, latent heat ($Q_{releaseed}$) is released from the wire, raising the temperature of the wire and its surroundings above the ambient temperature. For the duration that the wire is loaded, the latent heat flows from the wire into the copper disk, allowing the wire to cool. At state 3, the wire exits the bend and becomes unloaded, inducing the endothermic reverse transformation. Heat ($Q_{absorbed}$) is then absorbed by the wire and removed from the environment, decreasing the temperature of the surroundings from its initial condition and creating a cool space. At state 4, the now warmer wire continues to cycle around the apparatus. Heat is recovered from the surroundings, and the wire returns to state 1,

unloaded and at ambient temperature. This cycle can function both as a refrigerator and as a heat pump. In one respect, heat is being pumped into the copper disk at state 2. Conversely, heat is being removed from the environment as the wire at state 4 travels around the drive disk returning a state 1, exhibiting a cooling effect on the room.

Performance metrics

We consider three performance metrics in this work: (1) the cycle cooling power, (2) endothermic temperature change, and (3) the COP.

Cooling power ($Q_{absorbed}$) refers to the amount of heat absorbed from the environment by the wire once the wire becomes unloaded, at the exit of the bend (state 4 in Figure 2). In an isolated and ideal condition, if the wire were to take on a certain strain, and then recover that same strain (one loading-unloading cycle) at its transition temperature, the amount of heat released in the exothermic reaction must be completely removed in order to maximize the heat absorbed in the endothermic reaction.Thus, the maximum latent cooling power in a single cycle is limited by the heat removed from the wire (by means of conduction into the disk) after the initial exothermic reaction.Then, the heat absorbed in the endothermic reaction must be removed from the environment rather than the wire, in effect cooling the surroundings down. For this work, Q_{cool} will refer to the heat effectively removed from the disk.

In summary, cooling power depends on (1) the amount of material undergoing transformation (more reactions mean that more heat is released and absorbed) (2) the ability to fully remove heat from the wire before it becomes unloaded and (3) parasitic heat loss between the hot and cold sides of the cycle.

The endothermic temperature change is the difference between the initial ambient temperature and the resulting drop in temperature when heat from the environment as the wire becomes unloaded.

The COP, as described by equation 1, is a relationship between the desired output of the cycle (cooling power) and the power input necessary to achieve it. The higher the COP, the more efficient the system. It is in the interest that an ideal cycle will achieve the greatest amount of cooling power that largely outweighs its cost in power. For this cycle, power is defined as the rate of work required to plastically deform, or bend, the wire over time. The maximum possible cooling power is inherently linked to the amount of material sufficiently strained.

Potential for Improvement

Bending-mode cycles utilizing this technique have produced COPs as high as 3.5 and endothermic temperature drops of up to 8.95°C for strain rates between 0.01 s^{-1} and 0.025 s^{-1} [14]. Compared to elastocaloric cycles operating exclusively in uniaxial tension, the bending-mode cycle was able to significantly reduce the actuation force required to induce the right amount of strain, thereby

increasing the cooling power produced relative to the input power. This compares favorably with current HFC vapor-compression system COPs, which, at small power scales, have an upper limit of 3 [1].

Though these initial results represent a significant advancement in the development of elastocaloric heating and cooling technologies, there remains potential to further improve the cycle's performance. The largest concern is that there is a lack of knowledge of how several different parameters impact heat absorption into and out of the system. For instance, the cycle described above was characterized using a NiTi material having an energy density of only 7.52 J/g, when other studies have indicated that this value can be as high as 32 J/g [13], [14], [15]. If the design parameters and material properties of the cycle are optimized, maximized values of COP can potentially be achieved. Therefore, it is crucial that studies of how these parameters interact with each other in operation are pursued.

II. Methods

Analyzing the parameters of the bending mode flow loop cycle involved constructing and understanding two complimentary models: 1) a numerical simulation built using COMSOL Multiphysics v. 5.5, and 2) a physical apparatus to validate that the simulation can accurately reflect the thermal and mechanical behaviors observed. The numerical model was used to expand the cycle analysis past the physical limitations of the constructed apparatus. This was done by performing a parametric sweep on the system-- whereby the model simulates the cycle under numerous combinations of major parameters that allow us to establish parameter-result relationships.

III. Experimental Design Process and Setup

For this study, the new apparatus was designed to achieve the same fundamental experiments that the ARL cycle could run. Additionally, the parts were made to be more readily interchangeable to test specific sets of parameters. Other design considerations based on challenges encountered by Sharar (as indicated in the literature) are summarized in Table 1 [14].

ARL Flow Loop Challenges	Design Considerations
IR camera temperature measurements were taken directly on the moving NiTi wire in operation.	The copper heat exchanger tube will be replaced by a copper disk. Because the thermal properties of copper are known, using the IR camera to determine the average temperature of the disk will allow us to understand how heat moves from the wire to other materials and will also provide measurements that are more consistent and

	uniform.
The copper tube heat exchanger was fixed in place, resulting in potential heat generation due to rubbing friction between the wire and exchanger.	The copper disk will be free to rotate with the wire to prevent rubbing friction. Rotation is achieved by running the disk shaft through two 8 mm bearings and pillow blocks.
Heat was lost to the surroundings due to imperfect surface contact between the wire and the disk.	Wire cross sectional geometries that increase surface area contact will be considered. Additionally, the copper disk will have a groove fitted to hug the different wire samples so that the NiTi is flush against the copper.

Table 1: Previous challenges encountered while testing the ARL flow loop and respective design considerations.

With these design considerations, the resulting apparatus was constructed according to the sketch in Figure 4.

Figure 4: Elastocaloric flow loop apparatus design sketch.

In Figure 4, the left side of the apparatus consists of the copper disk, sized to achieve a bending strain of 1-2%. The disk itself is attached to a carrier that slides along a dovetail rail, which can easily be fixed to an optic table. The right side of the apparatus consists of the stepper motor and a PVC driving disk. A 6 rpm precision spur gear motor powered the drive disk and provided wire speed control by adjusting the voltage input. The disk and carrier system freely translate in the x-direction (forward or away from the motor and driving disk) and z-direction (vertically up and down) to ensure that wire contact and tension is appropriately maintained on both disks. Rail platform positioners attached to both the horizontal and vertical rails allow for precision

positioning and the ability to return quickly to a particular setup if adjustments are made or the cycle is disassembled.

To accommodate different wire cross sections and sizes, the drive disk was constructed with a radius of 15 cm to ensure that for wire diameters of 1-3 mm, the NiTi is not critically strained as it curves around it. Additionally, the drive disk was fabricated such that it had grooves that could hold round wires or flat wires, as shown in Figure 5.

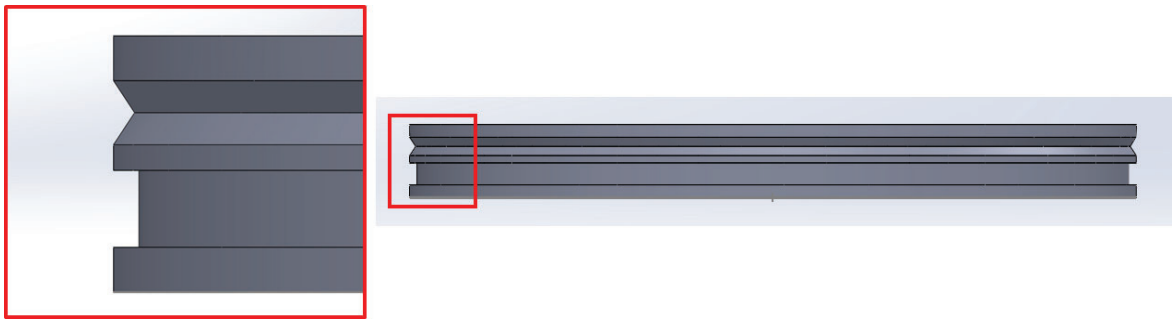

Figure 5: PVC drive disk round wire and flat wire grooves.

This design allowed more flexibility to readily test different wire geometries.

The final design (as drawn in SolidWorks) of the copper disk carrier is shown in Figure 6.

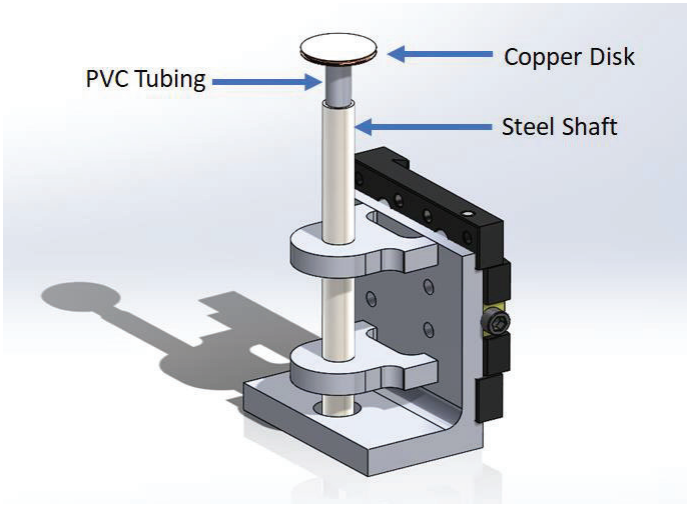

Figure 6: Finalized design of the disk-carrier apparatus.

The carrier consists of an interchangeable copper disk, PVC tubing, and a rotating steel shaft. The copper disk has a thin cylindrical stem that press-fits into the PVC tubing from the top. The steel shaft is shouldered down from a diameter of 8 mm to a diameter of ¾" for a length of 5 mm. This small, shouldered down section of the steel shaft press fits into the PVC tubing from the bottom. The PVC tubing is a thin-walled sleeve that has an inner diameter of ¼" and an outer diameter of

¾”. This tubing has two primary purposes: (1) to provide stiffness to counteract the horizontal tensile forces of the wire on the disk, and (2) to thermally isolate the copper disk and wire from the potential effects of losing heat by conduction through the steel shaft. It is critical that these parasitic heat losses are minimized in order to obtain an accurate understanding of how heat travels to the copper exchanger. Because PVC has an extremely low thermal conductivity (about 0.190 W/m*K), less heat is transferred through it. Additionally, by choosing a thin-walled tube, the surface contact area between the disk and the tube is also minimized, isolating the system from the carrier.

The final assembly of the carrier attached to the vertical rail is shown in Figure 7.

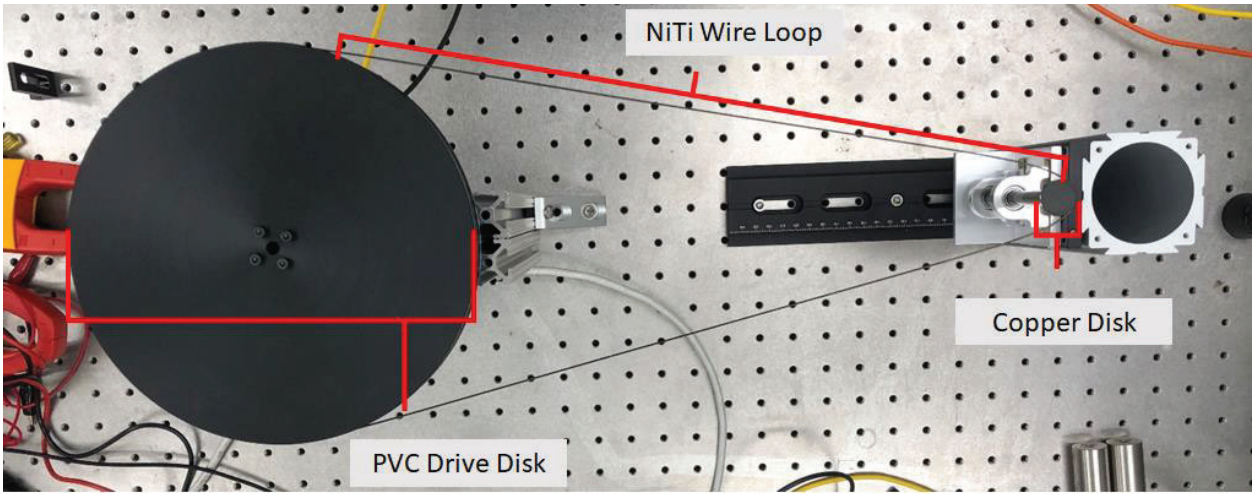

Figure 7: Experimental setup of elastocaloric flow loop apparatus built in Rickover.

Using this apparatus, an IR camera (FLIR SC8300 HD) was mounted above the copper disk to measure temperature changes and capture images and videos of the cycle in operation. The NiTi wire and copper disk were coated with graphite in order to increase their emissivity and produce more accurate temperature readings.

IV. Design of the COMSOL Model

The numerical model used to simulate the cycle was built using COMSOL Multiphysics (v. 5.5), a software capable of handling complex systems where multiple types of physics are at play. For this cycle, complexities are introduced primarily by the material properties of NiTi. Finding solutions to account for these behaviors ultimately drives the design of the model and how it is built. The model development process is outlined in the following steps:

1. Construction of model geometry
2. Characterizing motion of the wire and disk

3. Material selection
4. Describing how heat interacts in the system
5. Accounting for contact resistance
6. Accounting for convection

Construction of Model Geometry

The first step in building the model was to construct the system's components, according to the dimensions of the physical apparatus. Following the study conducted at ARL, the copper disk had a diameter of 18 mm, while the NiTi wire had a diameter of 1 mm [13]. These dimensions were calculated to maximize martensitic transformation in the wire, and subsequently, the heat release and absorption associated with it, and achieve above a critical strain of 1-2%.

Because the full refrigeration cycle takes place in between the inlet and outlet of the bending region of the wire (i.e. while transiting around the copper disk), only these areas of interest are modeled. Thus, the two major components of the cycle are the NiTi wire and the copper disk which it rotates around. Figure 8 shows the final geometry as modeled in COMSOL in comparison to the bending flow loop.

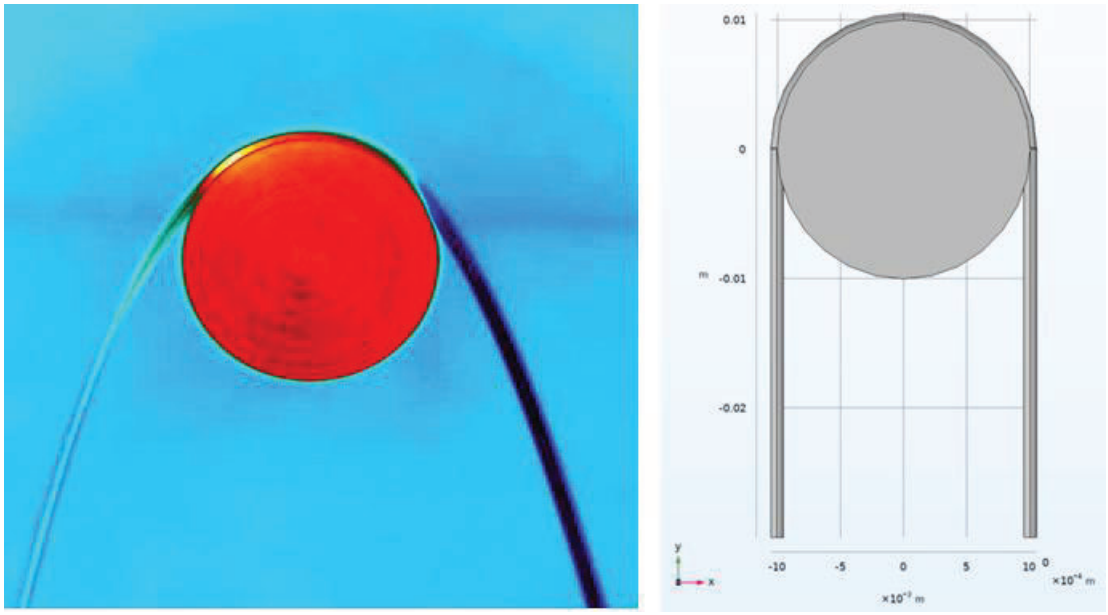

Figure 8: Final geometry of disk-wire system built in COMSOL.

Consistent with the physical design, the copper disk has a groove that hugs the wire of circular cross-section. For simplicity, the model assumes that the wire leaves at an angle of 0° to the y-axis. This assumption maximizes the arc length of contact between the bodies, but does not significantly affect the amount of heat transferred from the wire to the disk since the contact resistance was low in the experiment.

Characterizing Motion of the Wire and Disk

The next step was describing the motion of the wire rotating with the copper disk. At first glance, the system resembles a simple conveyor belt, which could easily be described in COMSOL Multiphysics using the Structural Mechanics Module, and assumes that both components are solids. However, because the material properties of NiTi are complex, particularly the strain-heat relationship, modelling the wire and disk as solids (limited by the modular nature of COMSOL) could not properly simulate how heat is released or moves throughout the system. Thus, in order to simulate the continuous flowing of the wire over the disk, and appropriately capture the loss of heat to its surroundings and the copper disk, both components are modeled as fluids rather than solids. Though modelling NiTi as fluid is unconventional, it is more critical to have the flexibility to allow specific thermal and mechanical behaviors to be mapped across the wire and disk. The next challenge was to then adjust the model to achieve linear-to-rotational motion as though it were a rigid body.

COMSOL solves two equations to govern the motion of fluids: the Navier-Stokes equation (Equation 2) and the continuity equation (Equation 3). For a compressible Newtonian fluid, or fluid in which its viscosity is linearly related to shear stress applied, these equations are as follow:

$$\underbrace{\rho\left(\frac{\partial \mathbf{u}}{\partial t}+\mathbf{u}\cdot\nabla\mathbf{u}\right)}_{1}=\underbrace{-\nabla p}_{2}+\underbrace{\nabla\cdot\left(\mu(\nabla\mathbf{u}+(\nabla\mathbf{u})^{T})-\frac{2}{3}\mu(\nabla\cdot\mathbf{u})\mathbf{I}\right)}_{3}+\underbrace{\mathbf{F}}_{4} \quad \textbf{(2)}$$

$$\frac{\delta\rho}{\delta t}+\Delta\cdot(\rho u)=0 \quad \textbf{(3)}$$

Together, these equations account for conservation of momentum and conservation of mass for a moving fluid, where u is the fluid's velocity, p is the pressure, T is the temperature, and μ is the dynamic viscosity. The Navier Stokes equation has four terms: the first term (1) relates to inertial forces, the second term (2) relates to pressure forces, the third term (3) relates to viscous forces, and the fourth term (4) relates to external applied forces on the fluid. This form of the Navier-Stokes equation describes laminar flow, and is the starting point for the wire and disk model.

To establish rigid body motion, incompressible flow is assumed, and the Creeping Flow module was implemented in COMSOL. Creeping flow describes flows characterized by extremely low Reynolds numbers, where the viscous forces of the fluid (molecular forces keeping them together) far outweigh the inertial forces driving them apart. This flow characterization best fits how a solid wire would behave, where each fluid molecule wants to move uniformly with the molecules around it. The implementation of incompressible flow and creeping flow neglects the inertial term (1) and parts of the viscous term (3), reducing the Navier Stokes equation to Equation 4:

$$0=-\Delta p+\Delta\cdot(\mu(\Delta u+(\Delta u)^{T}))+F \quad \textbf{(4)}$$

Using Equations 3 and 4, COMSOL interpreted the wire as an extremely viscous fluid flowing in a pipe.

Normally the fluid at the surface of the pipe has a zero velocity, but this is not the case for the wire. Thus, a slip condition was applied to the walls in order to keep the wire intact. Additionally, the dynamic viscosity of the fluids were driven to 0.

Once the wire and disk were made rigid, the final step was to define motion. A circular motion velocity field was applied to the curved section of the wire and the disk, while linear motion was applied to the straight sections of the wire. The circular motion and linear velocity fields are defined in Equations 5 and 6, respectively.

$$u_{rotational} = < -\dot{\theta}y, \dot{\theta}x > \quad \textbf{(5)}$$

$$u_{linear} = v_0 \quad \textbf{(6)}$$

$\dot{\theta}$is the angular velocity of the wire in rad/s and v_0 is the wire speed in mm/s.

The result of each of these adjustments was rigid body motion-- uniform flow across a plane, perpendicular to flow. Figure 9 shows the velocity gradient of the wire flowing around the disk.

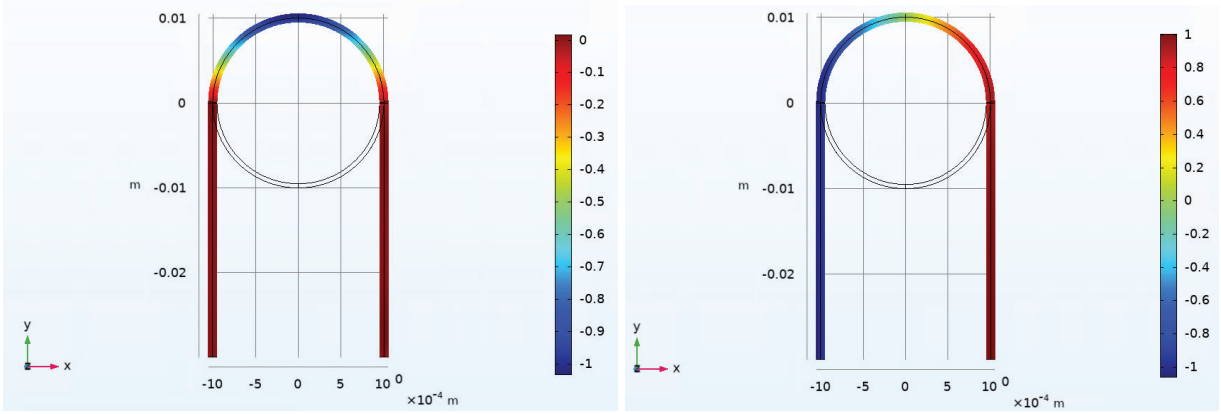

(a) (b)

Figure 9: Velocity gradient plotted over the NiTi wire. (a) x-velocity normalized over the magnitude of v_0. (b) y-velocity normalized over the magnitude of v_0.

Figure 9 shows that the wire moves as though it were a solid, flowing into the system with a positive linear velocity from the right side, entering the bend with continuous circular motion, and exiting with a negative linear velocity equal and opposite to the inlet.

Material Selection

Properties were manually input into COMSOL to match the thermal conductivity, electrical conductivity, heat capacity, and density of copper and NiTi, respectively.

Describing How Heat Interacts in the System

In order to model heat release in the wire, the system is designed under two primary assumptions: 1) Transformation of the NiTi takes place instantaneously; the sink and source are localized to only the regions entering and exiting the bend and are modelled as boundary heat sources (positive on one end, negative on the other). After which, heat conducts through the wire and into the disk. 2) There is no shift in the neutral axis as the wire traverses the bend. Thus, the strain distribution across the wire is simplified such that it is symmetrical (equal and opposite in value) above and below the center of the wire cross section. With these assumptions, Figure 10 shows the boundary surfaces where heat is released (highlighted in red) and absorbed (highlighted in blue). The inlet of this system is on the right side and has a positive heat source term to represent the exothermic reaction. Likewise, the outlet of the system is on the left side and has a negative heat term to represent the endothermic reaction.

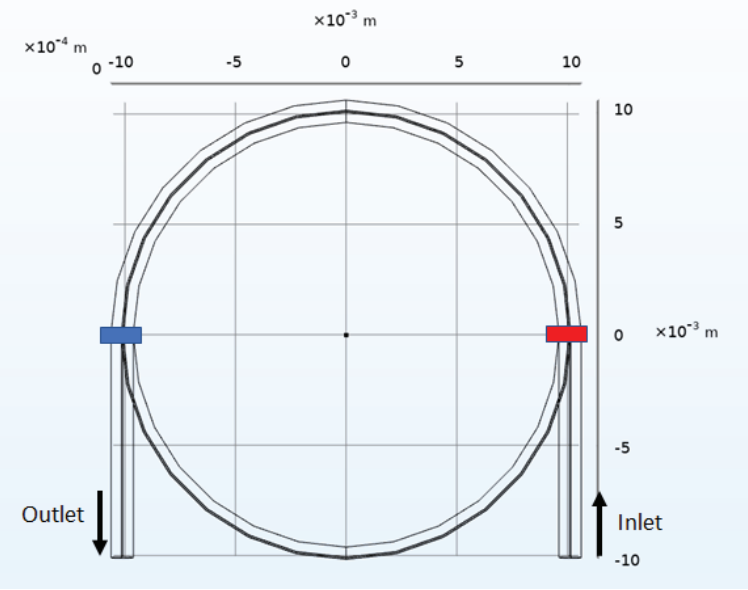

Figure 10: Surface boundary locations for equivalent heat flux terms

The quantity of heat released and absorbed is made up of two components: 1) the amount of work required to plasticize the wire above its critical strain (q_P, which then becomes heat) and 2) the latent heat (q_{Latent}) associated with martensitic transformation, as shown in Equation 7.

$$q = q_P + q_{Latent} \tag{7}$$

Calculating q_P

The first heating term is related to plastically working the wire. This work becomes heat and must be accounted for in the overall heat term applied to the wire. Plasticizing the material past critical strain (at about 1-2%) initiates the conditions for martensitic transformation, however it also

requires mechanical work to deform the material. To calculate this work, we quantify how much energy it takes to achieve this. Loading the wire depends on energy associated with applying the upper plateau of stress while unloading the wire depends on applying the lower plateau of stress. These values are calculated using force-strain data from experiments done at ARL, which demonstrated NiTi's asymmetric loading curve [15]. For simplicity, the data represented in Figure 2 is simplified to the curve illustrated in Figure 11, since only the values of the upper and lower plateaus (and their associated strain) contribute to the plastic work terms.

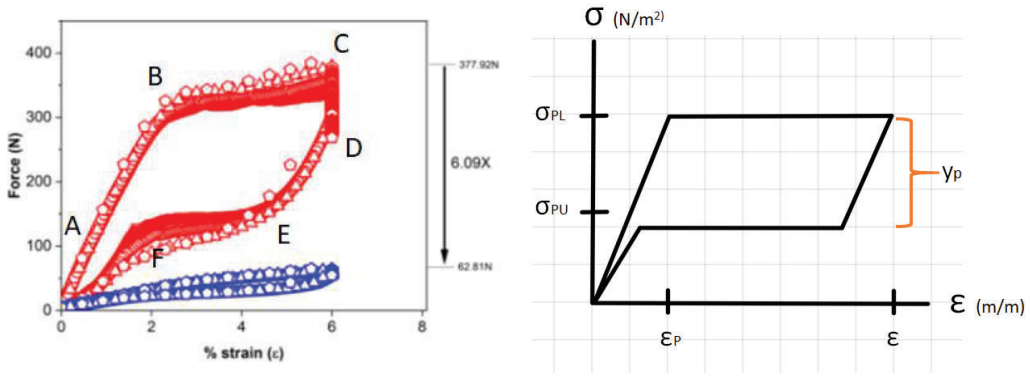

Figure 11: Simplified load and unload curve for NiTi wire in axial tension.

σ_{PL} is the stress required to plastically load the wire and σ_{UL} is the stress required to plastically unload the wire. ε_P is the plastic strain (or critical strain) where permanent deformation and martensitic transformation begin to take place. The linear region preceding ε_P indicates the elastic region of the wire, where deformation is naturally recoverable.

Additionally, because heat is only released where critical strain is achieved, only a fraction of the wire will undergo transformation. These areas of plasticization (heat releasing and absorbing sections of the wire) are modelled in Figure 12.

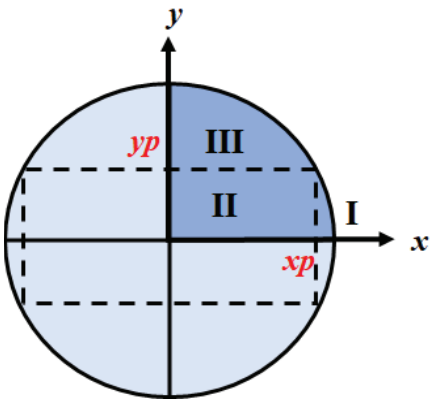

Figure 12: Plasticized regions of a NiTi wire cross section while experiencing a bending load, as modelled in COMSOL.

The region enclosed between y_p (the plasticized y-coordinate), x_p (plasticized x-coordinate), and the outer edge of the wire is the region of wire that is expected to be critically strained, and thus, heat absorbing and releasing. This critical region is referred to as Region III on the diagram. For computational purposes, the diagram shows this area in one quadrant of the cross section. However, this effect is symmetrical across the other three quadrants as well. We can then define exactly where this region is on the cross section depending on how strained the wire is. Using the material's elastic modulus (E), the radius of curvature of the wire bend (ρ), and Hooke's Law, y_p and x_p are calculated as follows:

$$y_p = \frac{\sigma_{PL}\rho}{E} \quad \textbf{(8)}$$

$$x_p = \sqrt{r^2 - (\frac{\sigma_{PL}\rho}{E})^2} \quad \textbf{(9)}$$

The energy required to load the wire is then obtained by integrating the area under the upper half of the curve from Figure 9 from ε_P to ε, taking only the plastic region into account and omitting the elastic region (since it is self-recovering). Likewise, the energy required to unload the wire is obtained by integrating the lower half of the curve. The results are as follow in Equations 10 and 11:

$$U_{PL} = \sigma_{PL}(\varepsilon - \varepsilon_P) \quad \textbf{(10)}$$

$$U_{UL} = \sigma_{UL}(\varepsilon - \varepsilon_P) \quad \textbf{(11)}$$

For these cases, U is the energy required in J/m^3. In order to express these terms as the rate of work to plasticize a volume of wire over time, Equations 10 and 11 are multiplied by the wire speed (v_0), or flow rate of the loop. Then, by combining these with Equations 8 and 9, the resulting plasticized work terms (expressed as a heat flux) for loading and unloading the wire, respectively are:

$$q_{PL}'' = \frac{\sigma_{PL}v_0}{\rho}(y - y_p) \quad \textbf{(12)}$$

$$q_{PU}'' = \frac{\sigma_{PU}v_0}{\rho}(y - y_p) \quad \textbf{(13)}$$

Equations 12 and 13 calculate the resulting heat release in W/m^2 of NiTi transformed in a period of time.

Calculating q_{Latent}

The second heat term is associated with latent energy release and absorption due to martensitic transformation. This term, expressed as a heat flux (W/m^2), is as follows:

$$q_{Latent}'' = L\,\rho_{NiTi}\,v_0 \tag{14}$$

L is the latent heat, or energy density of the wire in J/kg. L is associated with the expected energy stored in the material. ρ_{NiTi} is the density of the wire in kg/m^3. V_0 is the linear initial velocity (wire feed rate) at the inlet and exit of the bend in m/s, or how much of the material (lengthwise) is passing through the boundary heat source per second.

By combining Equations 7, 12 (for the loading case), 13 (for the unloading case), and 14, the overall heat implementation for the boundary inlet and outlet of the wire system for loading and unloading the wire is:

$$q_{Load}'' = \frac{\sigma_{PL} v_0}{\rho}(y - y_p) + L\,\rho_{NiTi}\,v_0 \tag{15}$$

$$q_{Unload}'' = \frac{\sigma_{PU} v_0}{\rho}(y - y_p) - L\,\rho_{NiTi}\,v_0 \tag{16}$$

For these expressions, a positive value indicates a heat release while a negative value indicates a heat absorption. The heat from working, however, is positive in both the loading and unloading conditions because heat is produced in both cases.

The resulting heat distribution for the applied boundary with these implementations of heat are shown in Figure 13.

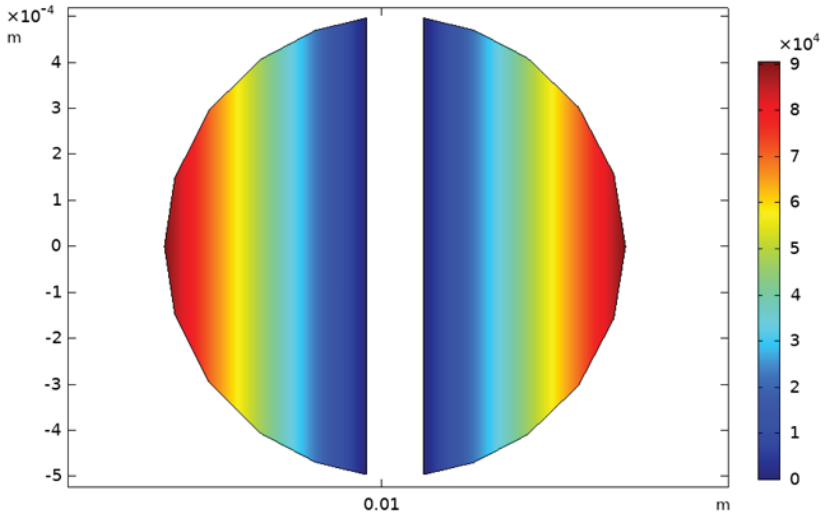

Figure 13: Heat distribution over the wire cross section of the inlet boundary (W/m^2).

Consistent with the theory and calculations, this resulting heat distribution correctly reflects the magnitude of heat released (which varies depending on strain) as well as where along the wire transformation occurs. The heat term is not implemented in the elastic region of the wire, where martensitic transformation does not take place.

Accounting for Contact Resistance

Thermal contact resistance has to do with the wire's ability to effectively conduct heat into the disk. Contact resistance is a result of asperities, or air pockets, present in between two contacting materials associated with the roughness of the materials. Figure 14 illustrates the roughness between materials and resulting asperities.

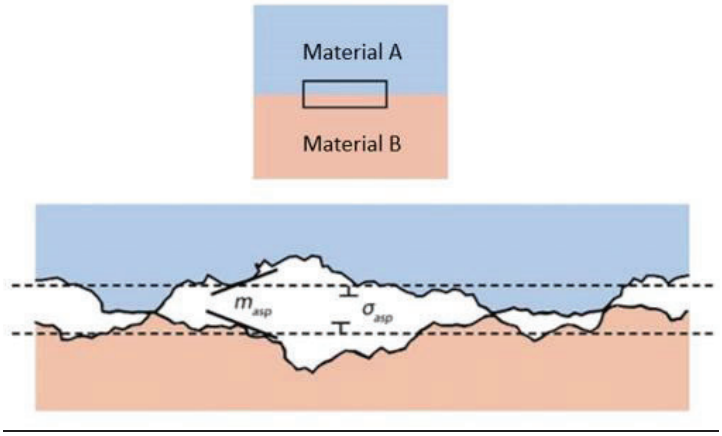

Figure 14: Surface roughness between two contacting materials.[1]

Though these asperities exist at the micro and nano scale levels, they have a significant impact on effective conduction between their surfaces. For any contacting metals, the thermal conductivity of gases (usually air) is much smaller than that of the metals. Thus, imperfect contact due to surface asperities result in less heat transferred by conduction between the two surfaces, creating an insulating effect.

COMSOL models the thermal contact resistance, a thin layer material of negligible thickness applied over the contacting surfaces, as highlighted in Figure 15.

[1] Image obtained from: https://www.comsol.com/blogs/thermal-contact-resistance-simulation/

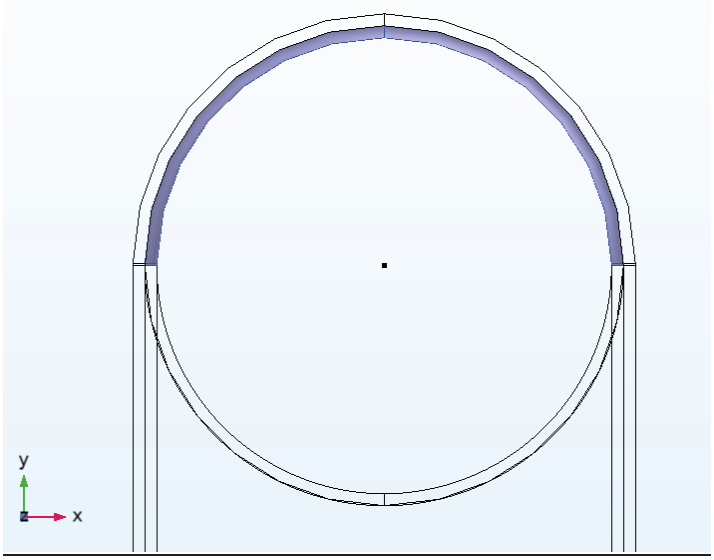

Figure 15: Contacting surface between the copper disk and Niti wire.

Accounting for Convection

Convection heat transfer is the means by which heat leaves the disk and escapes to the surroundings. There are two types: forced convection and natural convection. Forced convection occurs when heat is transferred due to the motion of a fluid, while natural convection occurs due to the buoyant forces that accompany a density gradient that exists in a fluid (i.e. the air around the system). Because the rotation of the disk does not operate at high speeds, natural convection is assumed to be the dominant mode of heat transfer that removes heat from the disk. However, the values of the convection heat transfer coefficient applied to the disk ranged from those expected for free convection to forced convection.

$$q_{Cool} = h\,A_s\,(T_{disk} - T_\infty) \qquad \textbf{(17)}$$

q_{Cool} is the heat leaving the disk in Watts. h is the convection coefficient ($W/m^2 \cdot K$), which depends on the geometry of the heated body, its orientation, and the characteristic fluid flow around it. A_s is the total surface area of the disk (m^2). Lastly, T_{Disk} is the average temperature of the copper disk and T_∞ is the free stream, or surrounding temperature (both in K). Equation 17 is illustrative but the actual q_{Cool} was found by integrating over the disk surface area.

V. Results and Discussion

COMSOL Parametric Sweep Studies

With the model properly running, a series of tests were conducted in order to understand how each parameter in the system individually impacts the cycle's performance. These studies and their testing parameters are summarized in Table 2. For these tests, the ambient temperature is set to 293.15 K, or 20 °C.

Test	Wire Feed Rate v_0 (mm/s)	Wire Radius r (mm)	Radius of Curvature ρ (mm)	Convection Coefficient h ($W/m^2 \cdot K$)	Contact Resistance R_C ($m^2 \cdot K/W$)
1	↑	0.5 mm	9 mm	2.5 $W/m^2 \cdot K$	1e-04 $m^2 \cdot K/W$
2	5 mm/s	↑	9 mm	2.5 $W/m^2 \cdot K$	1e-04 $m^2 \cdot K/W$
3	5 mm/s	0.5 mm	↑	2.5 $W/m^2 \cdot K$	1e-04 $m^2 \cdot K/W$
4	5 mm/s	0.5 mm	9 mm	↑	1e-04 $m^2 \cdot K/W$
5	5 mm/s	0.5 mm	9 mm	2.5 $W/m^2 \cdot K$	↑
6	↑	0.5 mm	9 mm	2.5 $W/m^2 \cdot K$	↑
7	5 mm/s	0.5 mm	9 mm	↑	↑

Table 2: Parametric Sweep Testing Conditions.

Test 1: Effects of Wire Feed Rate (v_0)

While holding all other parameters constant, a parametric sweep was performed on COMSOL to vary the wire feed rate from a speed of 0.1 mm/s to 100 mm/s. The following plot was produced:

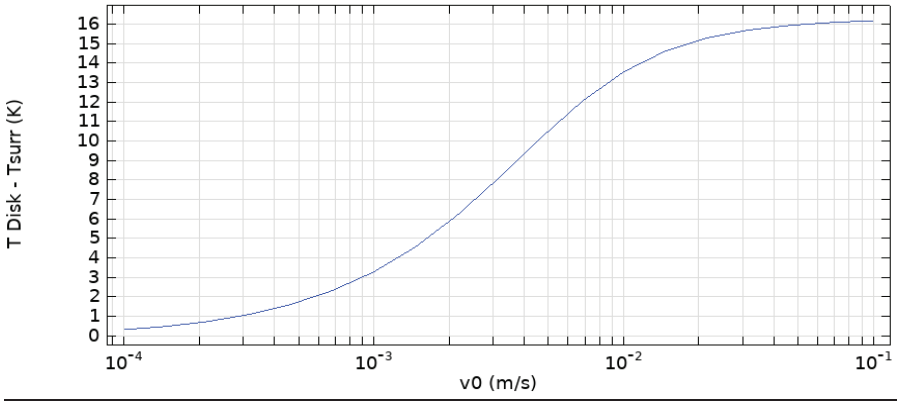

Figure 16: Wire feed rate (m/s) v. change in average disk temperature (K).

Figure 16 exhibits a positive trend between increasing wire speed and increasing average change in disk temperature (compared to the surroundings). Because the heat released over a period of time is directly proportional to the wire speed (Equations 14 and 15), or amount of wire being plastically loaded, it is expected that heat released and absorbed must increase with v_0. This would account for the initial increase in disk temperature for wire speeds below 10 mm/s -- more heat is released by the wire and can transfer into the disk.

However, the plot also exhibits a threshold at wire speeds greater than 1e-02 m/s, at which increasing the speed results in a temperature plateau. This shows that despite more heat being released from the wire as the disk increases in temperature, less heat is transferred to the disk and more heat remains in the wire. In the absence of any heat loss from the wire, the wire temperature would reach a maximum value on the bend. The plateau is below the adiabatic temperature rise due to back conduction and parasitic losses between the hot and cold side of the device.

Test 2: Effects of Wire Radius (r)

The next test varies the radius of the wire while holding the other parameters constant. Note that the thickness of the copper disk must increase with the wire radius in order to maintain grip. In this model, the disk thickness is calculated to be three times the radius of the wire. Thus, as wire radius increases, the mass of copper also increases, which impacts how much energy it takes to raise its temperature. Figure 17 shows the relationship COMSOL obtained between the wire radius and change in average disk temperature.

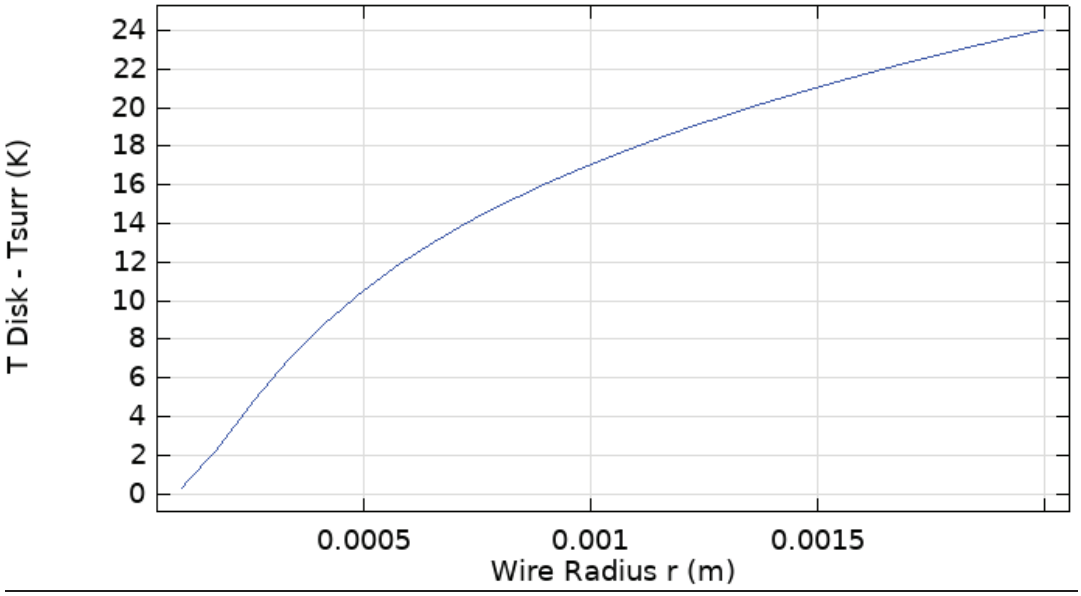

Figure 17: Wire radius (m) v. change in average disk temperature (K).

The positive trend in Figure 17 supports that increasing the wire radius and subsequently, the amount of material undergoing transformation, will result in more heat transferred into the disk and effectively raise its temperature.

Test 3: Effects of Radius of Curvature (ρ)

Figure 18 shows the relationship between the change in disk temperature and the disk radius.

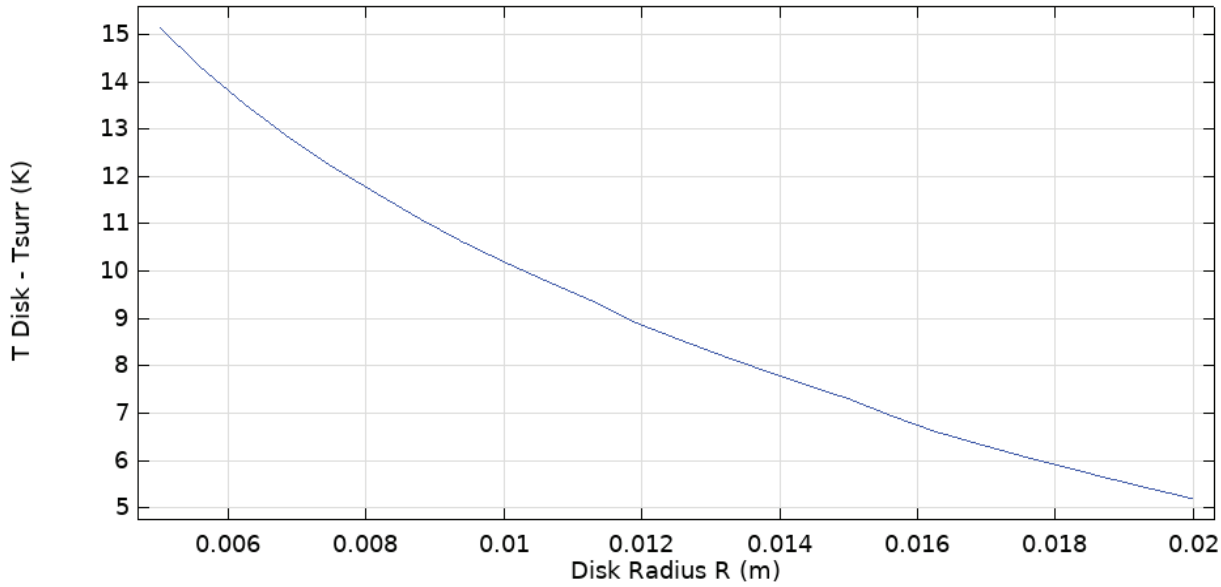

Figure 18: Disk radius (m) v. change in average disk temperature (K).

The radius of curvature, or disk radius, affects the strain distribution of the wire. Where strain is defined as the ratio of the wire radius to the radius of curvature (r/ρ), increasing the disk radius will decrease the maximum strain that the wire can experience. This would limit the amount of martensitic transformation able to take place. Figure 18 reflects this negative correlation. The greater the radius of curvature, the less heat is released from the wire and absorbed by the disk, resulting in smaller temperature changes.

Test 4: Effects of Convection Coefficient

Figure 19 shows the temperature change for the disk as the convection coefficient increases.

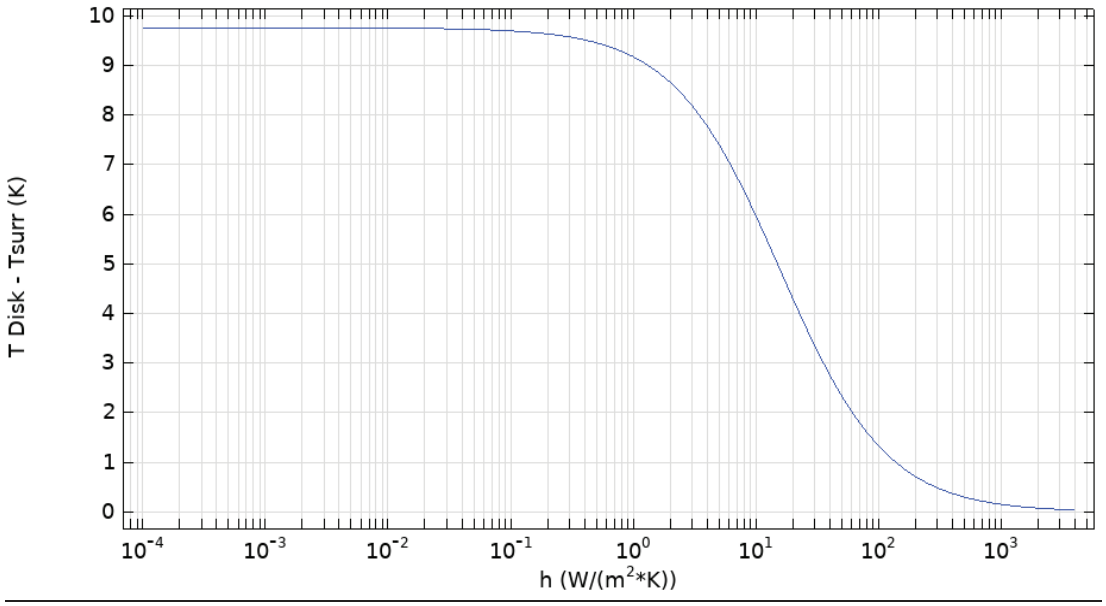

Figure 19: Convection coefficient (W/m^2·K) v. change in average disk temperature (K).

Figure 19 reveals that low convection coefficients (corresponding to low convection heat transfer off the disk surface) exhibit little effects on the steady state temperature of the disk. For the conditions outlined in Table 2, heat is not noticeably removed from the disk until the convection coefficient becomes greater than 0.1W/m^2·K. For *h* greater than 1 W/m^2·K, Figure 19 shows a negative trend in disk temperature for increasing convection coefficient. This is because at greater *h* values, heat is more readily able to be removed from the disk. Thus, as convection increases, less heat is retained by the disk, and the overall change in temperature of the disk decreases, approaching zero.

Test 5: Effects of Contact Resistance

The relationship between contact resistance and disk temperature are plotted in Figure 20.

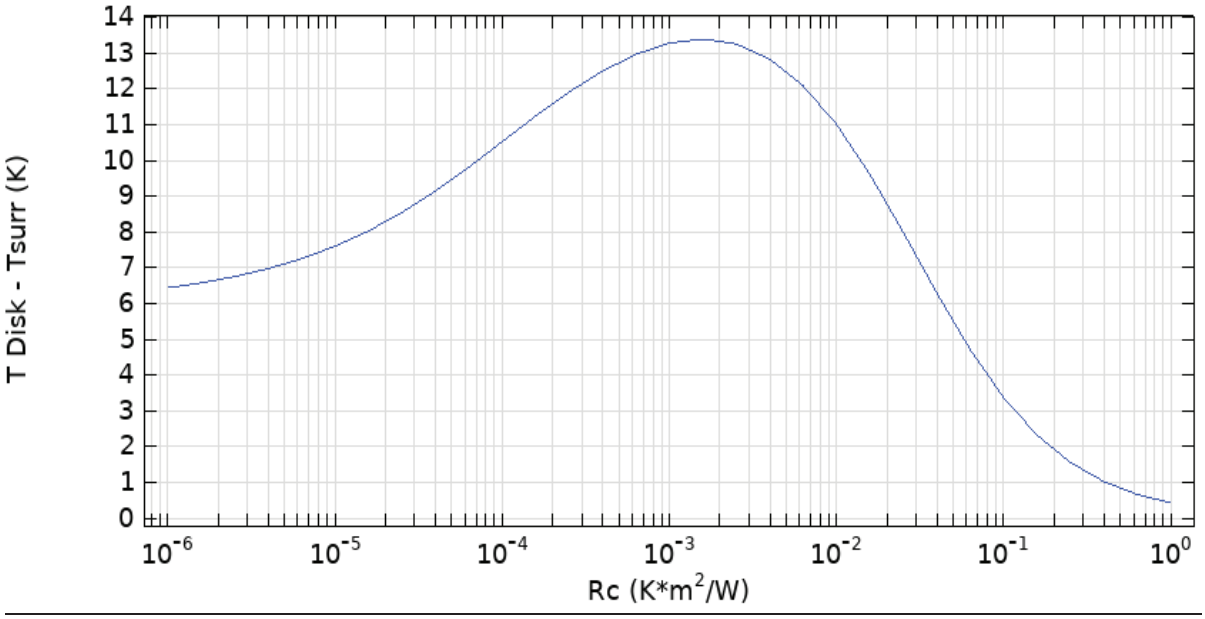

Figure 20: Contact resistance (m^2·K/W) v. change in average disk temperature (K).

The thermal contact resistance indicates how well heat can conduct between the wire and the disk. For low contact resistances, more heat is able to conduct from the wire into the disk, resulting in the initial positive trend between resistance and disk temperature. Generally, as contact resistance increases, it becomes more difficult for heat to transfer between the bodies. At the maximum contact resistance, the wire and disk are essentially insulated from each other, driving conduction heat transfer,and thus, the change in disk temperature to zero. Figure 20 reveals that there exists an optimal amount of contact resistance to maximize heat retained by the disk.

Test 6: Parametric Sweep Varying Wire Feed Rate and Contact Resistance

A parametric sweep was performed to understand how changing the contact resistance affected the trends observed for cycle performance at increasing wire speeds. The results for how these parameters affected COP, cooling power, and change in disk temperature are plotted in Figure 21.

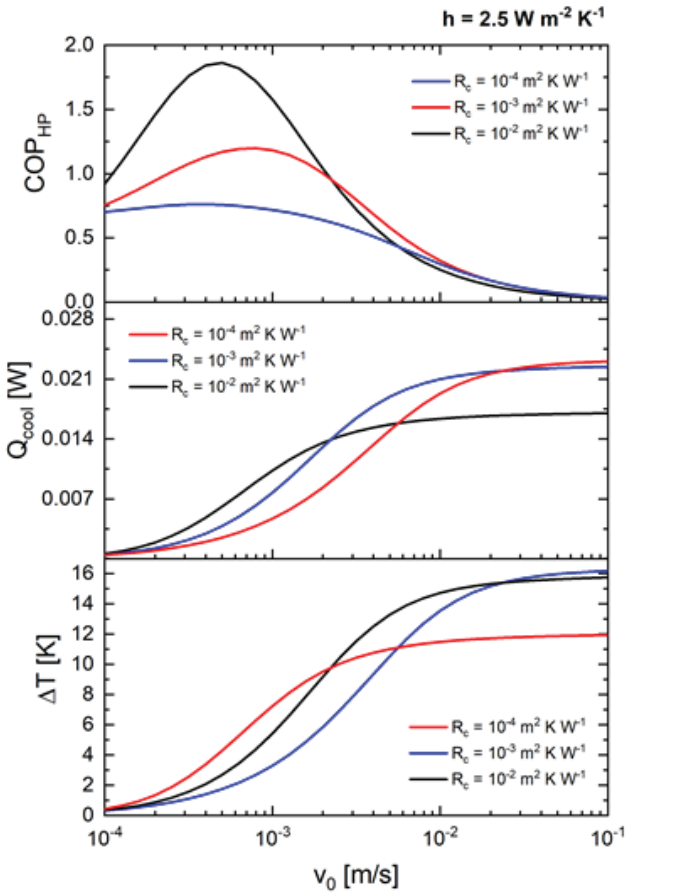

Figure 21: Wire speed (m/s) v. COP (top), cooling power (middle), and change in average disk temperature (bottom) for varying contact resistances.

The plots of cooling power and disk temperature show trends similar to the trend demonstrated in Test 1. For each contact resistance, an increasing wire speed will initially increase the heating and cooling effect of the cycle. However, at high speeds the increased heat absorption does not have time to effectively transfer into the disk, resulting in a leveling off in both the cooling power and temperature as shown in Figure 21. The plots also show that the speed at which these values begin to plateau (where increasing v_0 becomes ineffective) shifts depending on the contact resistance of the system. This preliminary test suggests that for this range of contact resistance, it may be more advantageous to strive for a higher contact resistance in order to lower the effective wire speed to achieve higher cooling power.

The plot of COP against increasing wire speeds exhibit clear maximums for all three contact resistance cases. As the wire speed increases, the COP also increases. This is consistent with Equations 14 and 15 as well as Test 1, which show that heat release is directly related to wire speed increase. Thus, COP rises because the heat release/absorption terms also rise. This is also

consistent with the Q_{cool} and ΔT graphs. However, as the wire speed continues to increase, the COP reaches a maximum and starts to decrease. This is supported by the cooling power and temperature plots: as the wire speed increases, the cooling power eventually levels out, however the power to achieve greater speeds is still increasing. Thus, the work rate will outweigh the cooling power once the wire speed threshold is reached, and a maximum exists before that point. For increasing contact resistance, this trend increases in overall magnitude, with the greatest COP maximum achieved with the lowest contact resistance.

Test 7: Parametric Sweep Varying Convection Coefficient and Contact Resistance

A parametric sweep was performed to expand on the results of Tests 4 and 5 and gain a greater sense of how the cycle operates with varying convection coefficients and contact resistance. The convection coefficient was varied from 0 to 40 $W/m^2 \cdot K$ and the contact resistance was varied from 1e−06 to 1 $m^2 \cdot K/W$. Using these operating conditions, the COP and change in average disk temperature were plotted in Figure 22. Note that because the wire speed is constant (v_0 = 5 mm/s), the work input is also constant. Thus, the COP is also an indication of the cooling power.

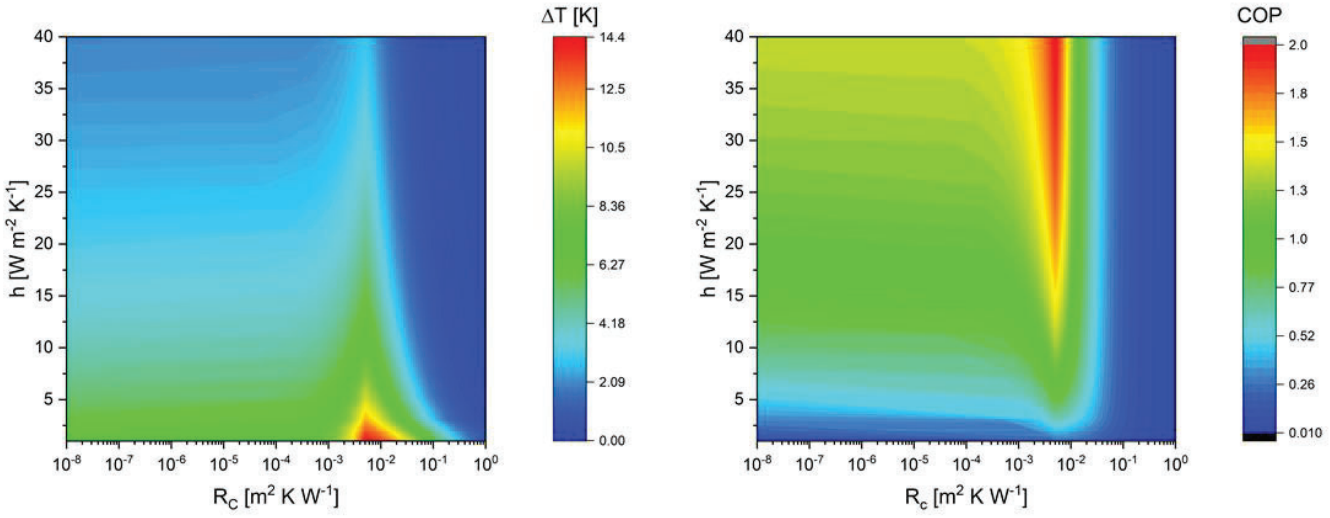

(a) **(b)**

Figure 22: Thermal contact resistance (x-axis) and convection coefficient (y-axis) contour plots. (a) Change in average disk temperature contour plot. (b) COP contour plot.

For both the disk temperature and the COP for this system, Figure 22 shows optimal ranges for certain combinations of contact resistance and convection coefficient. Consistent with Test 4, increasing the convection coefficient makes it easier for heat to escape the disk. Thus, the change in disk temperature tends toward zero and the COP increases (because the more heat is removed from the wire and disk system, the greater the cooling capacity of the cycle). Consistent with Test

5, as contact resistance increases, the wire and disk become more insulating, and the change in disk temperature decreases, tending toward zero. The optimal points, however, reveal an interesting relationship between the disk temperature, COP, and contact resistance.

Decreasing the contact resistance makes it easier for heat to conduct between the bodies. This allows more heat to enter into the disk through the hot inlet of the bend, effectively removing it from the wire. However, this also allows heat to escape through the cold point of heat absorption at the flow outlet, effectively diminishing the cooling effect. Thus, if the contact resistance is too low, the cycle does not perform as effectively.

Increasing the contact resistance makes the bodies more insulating. Less heat can enter the disk as the wire initially releases heat. However, the wire still has the remaining arc length of the contact space to give its heat to the disk. At the point of heat absorption, however, the higher contact resistance prevents heat transferring into the cold point on the wire, preserving the cooling effect.

Thus, Figure 22 reveals that for this flow loop, an optimal combination of contact resistance and heat removed via convection heat transfer exists.

Experimental Results

Using the IR camera, the study was expanded to the physical apparatus to gain a better understanding of the expected temperature changes of the system. Figure 23 captures the cycle running after 200 seconds. The wire speed was 5.2 mm/s, the wire radius was 0.5 mm, and the disk radius was 9 mm.

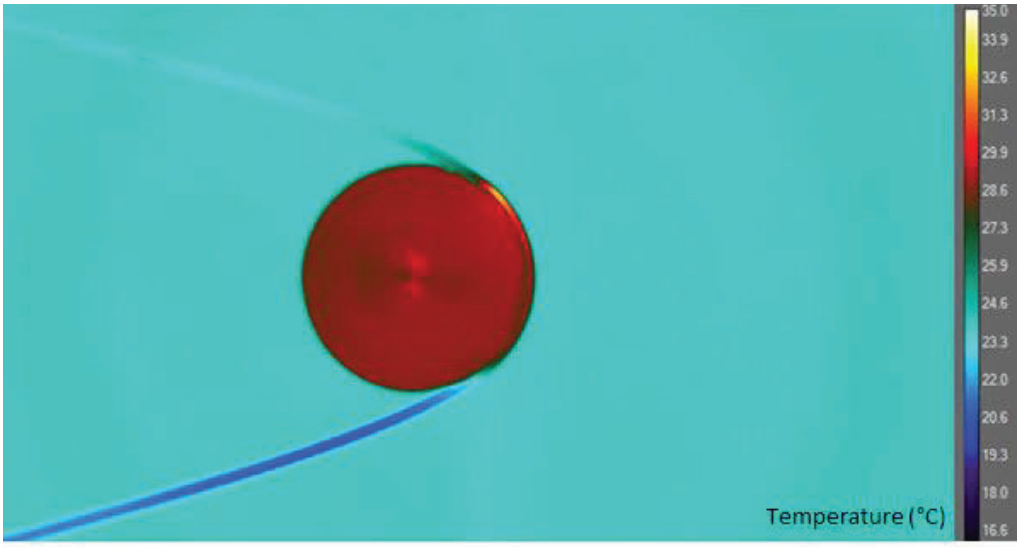

Figure 23: IR image of the elastocaloric flow loop.

Mimicking this study with the same parameters in COMSOL, a simulation at steady state was run in order to draw comparisons and match convection coefficient and contact resistance operating conditions. The results are summarized in Table 3.

Temperature (°C) (T_{Surr} = 23 °C)	Experiment	COMSOL model
Disk (average)	29 °C	30.95 °C
Wire Inlet (hot)	31.5 °C	27.75 °C
Wire Outlet (cold)	20.6 °C	20.74 °C

Table 3: Experimental and computational temperature comparisons for a steady state system

For the COMSOL model, the convection coefficient and contact resistance used were 4 $W/m^2 \cdot K$ and 1.5e-04 $m^2 \cdot K/W$, respectively. These values were estimated based off of the contour plots in Figure 22. Though the experiment and COMSOL model do not align perfectly, the model was able to predict the steady state temperature within an upper value of 3.75 °C and a lower value of 0.14 °C. Consistent with the experiment, the COMSOL model exhibited heating to above the ambient temperature at the hot wire inlet and cooling below the ambient temperature at the cold wire outlet. Unlike the physical test, the simulation did not predict a wire inlet temperature greater than the average disk temperature at steady state. Further accuracy in the convection coefficient and contact resistance would contribute to closer values between the computational and physical experiments.

VI. Conclusion

This study explored the parametric space of an elastocaloric refrigerator/heat pump, which had shown promising potential for improvements in COP, temperature change, and cooling power for applications in small scale refrigeration. A simulation of the elastocaloric flow loop was constructed from the ground up using COMSOL Multiphysics v. 5.5 and was shown to demonstrate the physical and thermal behaviors of the actual system. Using this model, several parametric sweeps were performed to understand the effect that wire speed, wire radius, radius of curvature, convection coefficient, and contact resistance each had on the system's performance, and how certain combinations affected it. Surprising trends were uncovered between the contact resistance and convection coefficient that increased our understanding of the cycle's behavior. There is hope of further understanding the performance tradeoffs with the continual development of the COMSOL model as testing expands deeper into both existing and new parameters, and the possibility of validation exists with the physical model.

VII. References

[1] W, Goetzler, R. Zogg, J. Young and C. Johnson, “Energy savings potential and RD&D opportunities for non-vapor-compression HVAV technologies,” U.S. Department of Energy Building Technologies Office (BTO), 2014.

[2] S. Fähler, U. K. Rößler, O. Kastner, J. Eckert, G. Eggeler, H. Emmerich, P. Entel, S. Müller, E. Quandt and K. Albe, "Caloric Effects in Ferroic Materials: New Concepts for Cooling," Advanced Engineering Materials, vol. 14, no. 1-2, pp. 10-19, 2012.

[3] B. Krevet, V. Pinneker, M. Rhode, C. Bechthold, E. Quandt and M. Kohl, “Evolution of temperature profiles duting stress-induced transformation in NiTi thin films,” *Materials Science Forum*, Vols. 738-739, pp. 287-291, 2013.

[4] B. Reedlunn, C. Churchill, E. Nelson, J. Shaw and S. Daly, "Tension, compression, and bending of superelastic shape memory alloy tubes," Journal of the Mechanics and Physics of Solids, vol. 63, pp. 506-537, 2014.

[5] K. Otsuka and C.M. Wayman, “Shape Memory Materials,”Cambridge University Press, pp. 27-49, 1998.

[6] D. Lagoudas, “Shape Memory Alloys: Modelling and Engineering Applications,” Springer Science and Business Media, pp. 1-23, 2008

[7] S. Qian, Y. Geng, Y. Wang, J. Ling, Y. Hwang, R. Radermacher, I. Takeuchi and J. Cui, "A review of elastocaloric cooling: Materials, cycles, and system integrations," International Journal of Refrigeration, vol. 64, pp. 1-19, 2016.

[8] F. Bruederlin, H. Ossmer, F. Wendler, S. Miyazaki and M. Kohl, “SMA foil-based elastocaloric cooling: from material behavior to device engineering,” Journal of Physics D: Applied Physics, vol. 50 no.42, pp. 1-4, 2017.

[9] Otubo J, Rigo O D, Coelho A A, Neto C M and Mei P R 2008 The influence of carbon and oxygen content on the martensitic transformation temperatures and enthalpies of NiTi shape memory alloy *Mater. Sci. Eng.* A 481–2 639–42

[10] Frenzel J, Wieczorek A, Opahle I, Maaß B, Drautz R and Eggeler G 2015 On the effect of alloy composition on martensite start temperatures and latent heats in NiTi-based shape memory alloys *Acta Mater.* 90 213–31

[11] Pieczyska E A, Tobushi H and Kulasinski K 2013 Development of transformation bands in TiNi SMA for various stress and strain rates studied by a fast and sensitive infrared camera *Smart Mater. Struct.* 22 035007

[12] Wang X, Xu B and Yue Z 2008 Phase transformation behavior of pseudoelastic NiTi shape memory alloys under large strain *J. Alloys Compd.* 463 417–22

[13] D. Sharar, J. Radice, R. Warzoha, B, Hanrahan, A. Smith, "Discrete Elastocaloric Cooling Using Low-Force Bending-Mode Actuation," Applied Physics Letters 118,184103, 2021.

[14] D. Sharar, J. Radice, R. Warzoha, B.Hanrahan and B. Chang, " First Demonstration of a Bending-Mode Elastocaloric Cooling 'Loop'," Proceedings of the Intersociety Conference on Thermal and Thermomechanical Phenomena in Electronic Systems, 2018.

[15] H. Hou, E. Simsek, D. Stasak, N. Hasan, S. Qian, R. Ott, J. Cui and I. Takeuchi, "Elastocaloric cooling of additive manufactured shape memory alloys with large latent heat," Journal of Physics D: Applied Physics, vol. 50, p. 10, 2017